The effect of materials on the designs of open flue low NOx burner with non-cooled burner surface

Liliana Matos
liliana.matos@tecnico.ulisboa.pt

Instituto Superior Técnico, Universidade de Lisboa, Portugal

November 2017

Abstract

There have been major concerns about pollutant emissions and this explains why the industries directly linked to these problems carry out their research in this direction. Domestic heating industry based on hydrocarbon fuels are under pressure from regulators to limit levels of harmful emissions such as NOx and CO. There are some commercialized solutions that reach low levels of polluting emissions, however it is important to develop simple and economically viable solutions that meet the limits imposed by legislation.

After analyzing the materials and working methods of domestic hot water appliances, focusing on atmospheric heaters that operate under the same principle as Bunsen burners, Cambridge Engineering Selector software is used to understand the benefits and limitations of each material and SimaPro to carry out a Life Cycle Assessment to understand which material has the lowest ecological footprint.

Using different materials, different flames are obtained and a morphological analysis is done to register how the variation of gas flow rate influence the flames for each Bunsen burner, then a spectroscopy analysis to estimate the equivalence ratio and a thermography analysis to find burner temperatures.

Finally, a simple 1D mathematical model is developed to predict air entrainment for a partially-premixed atmospheric burner.

With the results obtained, it is believed that the primary air does not change with the increase of temperature and that the buoyancy effect overlaps the effect of the heat transferred in the material.

Keywords: Self-aspirating burner, Primary air entrainment, Equivalence ratio, NOx emissions

1. Introduction

The topic of preventing pollutant emissions for the environment is not new, but in the last years, there has been a great concern about measures to avoid these emissions due to legislation that will be introduced in 2018.

As Costa and Coelho [1] stated in their book, this problem has received more attention from researchers, industries and governments, so it is therefore a natural commitment of the industrialized countries to legislate more restrictive limit values for NOx emissions.

Various types of combustion systems and burners have been studied due to the need of improving thermal performance and to reduce pollutant emissions, by developing the burner port geometry and the combustion system, as Hou et al. [2] and Jugjai and Rungsimuntuchart [3] did.

Talking about hot water heaters, it is possible to focus on the operation principle of a Bunsen burner, as it is most widely used. As Hou et al. [2] stated, this type is seen as a partially aerated burner that entrains primary air naturally carried out by the high velocity of the gas jet and ambient air, together. This primary air is mixed with the fuel gas before the occurrence of combustion.

Considering a Bunsen burner type, a self-aspirating cold burner type do not drag the same quantity of air as a hot one. During combustion, the burner heats up, because the flame transfers heat to the tube; the same happens with air/fuel mixture as the fuel exits the injector to form the flame.

As stated by Namkhat and Jugjai [4] the study of preheating effect caused by combustion allows the investigation of a self-aspirating burner. Also it allows to understand its operation mode and possible application to a heat recirculating combustion system for efficient energy. In order to achieve both improved thermal efficiency and reduced emissions of air pollutants, Zhen et al. [5] studied the effects of air preheat on the visual, thermal and emission characteristics in order to show that this technology of preheated air is one of the most useful and possibly implemented for domestic applications.

During this heating process, air/fuel mixture flow changes its properties (viscosity, density, velocity and others) and this leads to increased friction between the flow and the burner walls, so Reynolds number decreases, friction increases and the amount of entrained air decreases; this concept is usually called preheat effect. As it was written in the Patent No. 5 104 311 [6], the level of the primary air entrainment is of great importance for more complete combustion of the self-aspirating burners. Consequently, with the reduced air, NOx and CO emissions increase. For these reasons, there has been much research on this kind of burners.

Looking at the work done by Namkhat and Jugjai [4], where the purpose was to get a good understanding of the effects of changes in the combustion air temperature on the primary aeration and flame structure, they found that the primary aeration decreased with an increasing preheated air temperature. Finally, they recommended to take into consideration the preheating effect when designing the mixing tube and to obtain an accurate primary aeration.

Zhen et al. [5] experimentally investigated flames and they used a circular pipe burner to establish laminar Bunsen-type flame. They could relate NOx emissions with air preheated and found that NOx concentration increases as preheat temperature increases.

1.1. Materials and properties

To proof the preheat effect already stated above, it is possible to use different materials in a Bunsen burner, as they may have different performances when applying to the burner, according to their properties.

In most products available on the market, the most commonly used materials are stainless steel, copper, steel, brass and aluminium. Due to the knowledge of their mechanical and physical properties, these materials have been used for years as part of gas water heaters. Although aluminium has low melting points, they are widely used in these appliances, being constantly cooled through a system of water pipes.

Regarding material properties, there are some important ones to take into account when choosing materials to apply on this type of appliances, as thermal conductivity, temperature range, melting point, thermal expansion coefficient, density, high temperature resistance, among others.

To carry out some experimental tests, the materials mentioned above can be used and it is possible to study the hypothesis of using new materials, as alumina and silicon carbide.

2. Environmental assessment of materials

In order to present a detailed study on each mentioned material and focusing on the properties referred in previous section, two important analysis will be developed in order to find the materials that better fit the purpose of this work.

2.1. Using Cambridge Engineering Selector

In order to compare the materials stated above, regarding some properties already mentioned and in order to indicate what could be the best material to use, Cambridge Engineering Selector (CES) software was used, allowing the combination of engineering, economic and environmental properties [7].

With this software, it is possible to choose the materials to be compared according to some properties, make comparative graphs and analyze the relationships between the properties of each material. Materials properties charts are a great way to visualize and communicate materials properties [7].

Starting to focus on thermal conductivity (W/m.K), copper has the highest vaue for thermal conductivity (160-390 W/(m.K)) and stainless steel has the lowest (12-24 W/(m.K)).

Regarding the melting point, silicon carbide has the highest melting point (2000-2100 °C) and aluminum alloys have the lowest (465-677 °C). This property is very important, because it is related with the characteristic flame temperature, formed by the combustion of LPG with air. Considering stequiometry, adiabatic flame temperature for propane is 1970 °C (2243K - 2300K) [1].

Talking about thermal expansion coefficient, silicon carbide has the lowest value (4–4.8 μ

strain/°C) and aluminum alloys have the highest (21-24 μ strain/°C). This property may be important to ensure that the material does not change its shape when it reaches higher temperatures.

Regarding maximum service temperature, although silicon carbide has a small range of temperatures, it has the highest maximum service temperature (1400-1700 (°C)), while aluminum alloys have the lowest (120-210 (°C)).

Finally, regarding the price it is clear that alumina is the most expensive material (13.3–20.1 €/kg) and stainless steel is the cheapest material (6.07–6.68 €/kg).

Even knowing that only these characteristics are not sufficient to determine the material to use, it is possible to conclude that, probably, silicon carbide is the material that better fits the purpose of this project. Despite the high price, it has a good thermal conductivity, the highest melting point, the lowest thermal expansion coefficient, the maximum service temperature and a medium price comparing to the other materials.

2.2. Life Cycle Assessment

In order to complement the analysis done with CES software, with a Life Cycle Assessment it was possible to add another analysis feature and thus improve the conclusion on the material(s) to use.

The purpose of this study was to perform an environmental assessment of different materials already described in previous sections, with the aim to identify which of these materials had a greater impact on the environment. When doing such an analysis, it is necessary to define a functional unit, which was defined as 1 kg. The aim of this study was to perform a cradle-to-gate environmental assessment, considering that the material was received ready to use, without the need for any additional process, being the manufacturer responsible for the recycling and recovery process.

To perform inventory analysis, the data was compiled directly from the SimaPro database, considering the great majority of processes and its inputs and releases.

SimaPro is a decision support tool with the objective of monitor and measure the environmental impacts of each material [8]. For this reason, some impact categories were considered (Climate change, ozone deletion, marine eutrophication, human toxicity, metal depletion, fossil depletion and others). Each sample used in the experimental tests was previously weighed to carry out this analysis.

The method to apply a Life Cycle Assessment is midpoint-oriented, that converts the emissions of hazardous substances and extractions of natural resources into impact category indicators at the midpoint level [9].

It was decided to select an egalitarian perspective, considering a 500 year timeframe, being a long term perspective it provides a further vision to the future and it is the most precautionary perspective [9].

It was concluded that the value of kg CO_2 equivalent is lower in the case of alumina (a new material tested), making this material more environmental friendly, taking into account the production processes and the quantity produced. The material less envionmental friendly is brass.

3. Mathematical Model

3.1. Burner geometry

Presented in Figure 1 is the Bunsen burner type with all the elements considered in this work. It is important to note that in this work some constituents of a gas water heater are not considered, such as the combustion chamber and the heat exchanger. So it were considered:

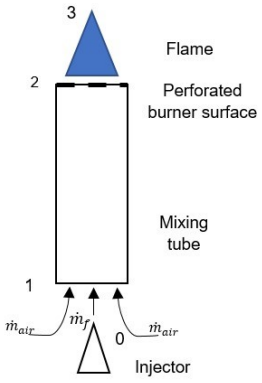

Figure 1: Bunsen burner geometry.

- Injector, which discharges a mass flow $\dot{m}_f$ of propane gas C_3H_8 through the entrance of the mixing tube (1);
- (1 to 2) Mixing tube with a circular cross section, with a specific diameter d, where a mass flow of entrained air $\dot{m}_{air}$ mixes with the fuel, originating a homogeneous mixture in the end of the tube (2);
- (2) Perforated burner surface where the flame is anchored;

- (3) Partially premixed flame where the air/fuel mixture is burned.

For the purpose of this work, the entrainment of a secondary mass flow of ambient air is not considered.

It is important to use a porous burner surface, as Keramiotis et al. [10] stated, because porous burners are characterized by low pollutant emissions, enhanced combustion stability across a wide range of conditions and the potential to operate in ultra-lean combustion regimes.

3.2. Assumptions and simplifications

The objective of the model was to predict the quantity of primary air entrainment into the burner. In order to achieve this objective, it was necessary to take into account the burner geometry, the ambient conditions and the gas flow.

The assumptions that will be considered for the model are: **1)** steady-state regime; **2)** the propane gas obeys the perfect gas law; **3)** the mixing tube is long enough in order to allow a perfect mixing between the fuel and the air; **4)** the flow is considered to be one-dimensional, means that the properties only change along the longitudinal direction; **5)** changes in potential and kinetic energies are ignored; **6)** combustion is complete.

3.3. Modeling of primary air entrainment

In this section will be presented the final analytic expression corresponding to the burner from position (0) to position (3). Some parameters should be considered when deriving the expressions for pressures at all these points.

To obtain the expressions of p_1 and p_2 it is necessary to resort to iterative processes, because in these points there is dependence of $\dot{m}_{air}$.

Burner model for primary air entrainment

In the model developed in this section, it is considered that the injector is discharging a certain mass flow rate of fuel $\dot{m}_f$ into the burner. Here the ignition of the mixture occurs and buoyancy effects $gV(\rho_{atm} - \rho)$ are considered between points (2) and (3).

Flow from the injector to the mixing tube entrance

In this first part of the stream considered, from the injector (0) through mixing tube entrance (1), the mass flow rate of fuel $\dot{m}_f$ is known and a mass of air from ambient air around the tube enters into the mixing tube in (1) – primary air. At that stage, this mass flow rate $\dot{m}_{air}$ is unknown and the model will be useful to compute this primary air stream.

The fuel mass flow exits the injector, which has a circular section, with a diameter d_{inj}, and the primary air enters the burner through the inlet of the mixing tube with a cross-sectional area of A_1, at a pressure p_1 equals to the ambient pressure. Temperature T_1 is considered, being the temperature registered at that point.

It is considered that the air flow is constant, adiabatic and incompressible, from the surrounding atmosphere to the point (1) and thus the generalized form of the Bernoulli's equation can be applied between points (0) and (1).

Flow at the entrance of the mixing tube and mixing of air/fuel inside the mixing tube

In this second part it was verified the entry of the mixture into the tube (1) and its propagation up to the point (2). Here the same conditions are considered, being the flow constant, adiabatic and incompressible, meaning that the generalized form of the Bernoulli's equation can be applied again to compute de pressure at the end of the mixing tube.

The mixture of air and fuel enters the tube, which has a cross-sectional area of A_1, and starts to propagate over a distance L, till the end of the tube in point (2), which also has a circular section with a cross-sectional area A_2 and it was considered that A_1=A_2.

In this step it is considered that the mass flow rate that entrains at the mixing tube is the same that reach the end of this tube, so $\dot{m}_2$=$\dot{m}_1$. Temperature T_1 is considered again and T_2 the temperature observed at the end of the tube.

Flow through the flame region

In the flame region, combustion occurs and flow changes the temperature, pressure, velocity, density and composition. The temperature at which combustion reaction occurs is admitted to be constant across the flame region. Temperature T_3 is the flame temperature. In this region it is important to introduce the momentum equation, considering it between points (2) and (3).

In the end:

$$p_0 + \frac{1}{2}\frac{{\dot{m}_0}^2}{\rho_{atm} A_1^2}(1 - k_{01}) = \frac{\rho_m A_2 (\frac{m_0 + m_f}{\rho_m A_1})^2 (\frac{\rho_m}{\rho_3} - 1) - gV_{23}(\rho_{atm} - \rho_3)}{A_2} + p_0 + \frac{1}{2}\frac{(\dot{m}_0 + \dot{m}_f)^2}{\rho_m A_1^2}(-1 - 1 - k_{12}) \quad (1)$$

The term k_{01} appears, representing the headloss coefficient that is highly dependent on the type of entrance considered. Typical values for this coefficient are present in Çengel and Cimbala [11], for different types of entrance. Is was assumed 0.5 as an input to the model.

The term k_{12} appears, representing the headloss coefficient that is dependent on the friction losses in the tube. Is was assumed 0.02 as an input to the model.

4. Experimental Setup

To validate the mathematical model derived in previous section it was necessary to perform some experiments in a simple prototype, Bunsen burner type. Three different tests were performed; a morphological analysis to specify the flame behavior for each tube, since the only variable manipulated by the user was the gas flow rate; a spectroscopy analysis to estimate the equivalence ratio of the flames considered; and a thermography analysis to find the temperatures at the beginning of the tube (1) and at the top, where flame was anchored (2).

All these tests were performed with the flame anchored at the end of the tube, thus were controlled by Lab View software (Alicate Scientific MC-1SLPM-D/5M for propane) to input a gas flow rate.

As already mentioned in the previous section, a perforated burner surface or quenching net was used, primarily to avoid flashback (i.e. to prevent the flame propagation towards the source of gas), but also to reduce pollutant emissions.

4.1. Morphological Analysis

In this first analysis, different tests were performed, and the objective was to understand the behavior of the flames by varying some key elements, as mixing tube internal and external diameter, consequently the surface area, and the tube material, keeping always the same height.

The gas flow rate in this test was varied between 0.1 and 0.6 standard liters per minute (SLPM), resulting in different flames for each tube and each flow. The photographic record of these flames was carried out with a Canon 500D.

Although the only input was gas, which enters the pipe through the injector, it was also considered a primary air entrainment that mixes with the gas along the pipe to form the flame at perforated surface.

Figure 3 shows the experimental setup used to perform these tests.

4.2. Spectroscopy analysis

In order to estimate the equivalence ratio of the flames considered in the previous analysis, a detailed analysis of the flame was performed using spectroscopy.

This analysis had a great contribution to the primary air entrainment computation, since the objective here was to estimate the equivalence ratio and, knowing the gas flow rate, easily the primary air entrainment is obtained. It is based on the chemiluminescence emission of the flame by recording the spectrum of flame emission between 250 and 575 nm by means of an Optics HR2000 High-resolution Miniature Fiber Optic Spectrometer.

In this method, an optical fiber was used at the flame in study and it was placed in such a way that their field of view contained a reduced flame volume using a slit opened by 0.20, 0.25, 0.50 and 0.75 mm, to ensure that the contribution of the flame was only from that fiber bundle.

A flame like the one in Figure 2 emits radiation mostly due to OH*, CH* and C_2^* radicals, approximately at 310, 430 and 515 nm, respectively. They appear in the course of reactions that occur during the combustion process, such as formation and dissociation reactions, and are important points to compute the equivalence ratio.

Figure 2: Flame observed in Tube 6 with flow rate 0.5 SLPM.

All spectra obtained in this test were averaged spectra for 50 s.

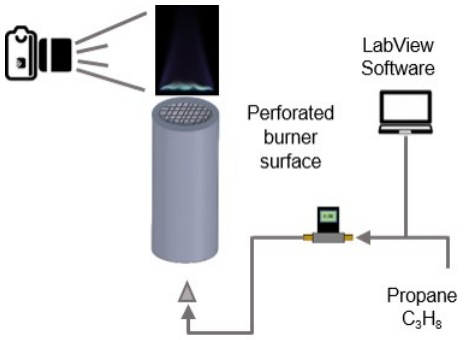

Figure 3: Experimental setup Morphology analysis.

4.3. Thermography analysis

As an input to the mathematical model, it was necessary to find the temperatures verified at the tube entrance (1) and at the end (2), where the flame was anchored.

In this test, temperatures were recorded using an infrared camera, an Onca-MWIR-InSb from Xenics that gives "images" of the temperature field of the object under study, having the ability to read the infrared radiation with its sensors. The result will be a two-dimensional temperature field with an accuracy of +/- 0.5°C. A camera software was used to record and process the data collected, according to a experimental setup similar to the one from Figure 3, but with an infrared camera instead a photographic camera.

With a camera pointed at the object, it was necessary to make a calibration for the desired distance with a black object. After this calibration, keeping the camera in the same position, it was possible to collect the temperature data.

Figure 4 shows the experimental setup used to perform these tests.

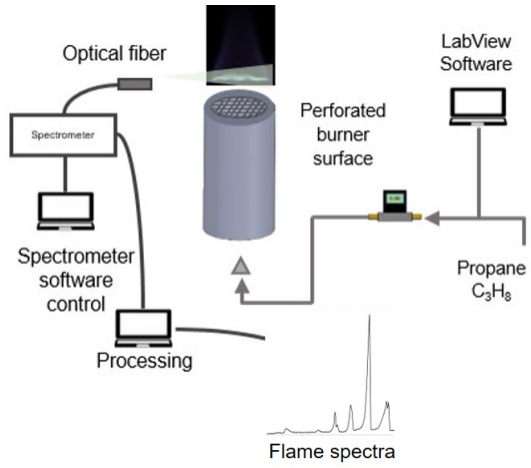

Figure 4: Experimental setup Spectroscopy analysis.

4.4. Uncertainty analysis

The uncertainty of the equivalence ratio and chemiluminescence results obtained is a consequence of the flow controllers, the spectrometer measurements and the data treatment.

Using the uncertainty associated with the flow measurement, the spectrum file and the calibration curves for calculating the equivalence ratio, is was concluded that all uncertainties verified were less than 10%.

4.5. Porous burner surface

Porous surface used is shown in Figure 5, it has been sized to the internal diameter of each tube and has a mesh having an area of 0.074 x 0.074 cm^2.

Figure 5: Porous burner surface used in all tests.

5. Results and Discussion

In this section, the results of the experimental tests performed in the Bunsen burner will be presented for the different types of analysis performed.

5.1. Morphological Analysis

As stated in previous section, morphological analysis was important to know the different types of flames that result from the use of different tubes varying some key elements such as mixing tube internal and external diameter and the tube material, keeping always the same height. From a large set of flames, two distinct flames were verified; one with a yellow tip and one with a flame with small oscillations near the perforated burner surface and a plume.

Figures 2 and 6 presents the flames for two of the tubes tested, with a gas flow rate of 0.5 SLPM.

Figure 6: Flame observed in Tube 1 with flow rate 0.5 SLPM.

With this analysis, it was decided to choose two different tubes to make the next proposed analysis. As the flames are quite similar from the tube 2 till 9, tubes 1 and 6 was chosen to perform spectroscopy and thermography analysis.

5.2. Spectroscopy analysis

In order to estimate the equivalence ratio of the flames considered in the previous analysis, it was

decided to perform a spectroscopy analysis of the flames.

To facilitate the analysis of these results, the spectroscopy study was divided into three different tests, representing three different approaches.

5.2.1 Spectroscopy I

In this first approach, tubes 1 and 6 were tested considering two different positions (A and B) for the optical probe for each tube, as it is possible to see in Figure 7, and a data collection time of 50 s.

In tube 1, the analysis was performed for two different gas flows rates, 0.25 and 0.50 SLPM. It was found that the results were very similar, so it was decided to present in Figure 8 the results for $\dot{m}_f = 0.50$ SLPM.

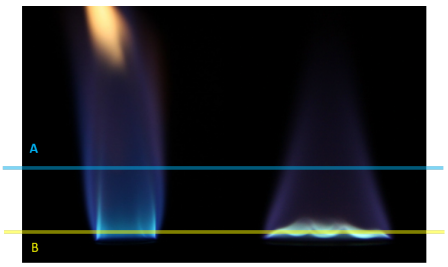

Figure 7: Two different positions considered for the optical probe.

In tube 6, for position A, the procedure was the same described for tube 1; for position B, a slit was considered in an attempt to restrict the capture of the optical probe to the zone of interest in the flame. Slits of 0.5 and 0.75 mm were tested. Figure 9 shows the results with a slit of 0.5 mm.

For both tubes, it is possible to see that probe position A it is not good to perform this analysis, due to the great contribution of CO_2^* broadband background radiation, as it is possible to see in Figure 8. For the probe position B, the flame emission spectra is better, but it is not possible to draw conclusions about equivalence ratio.

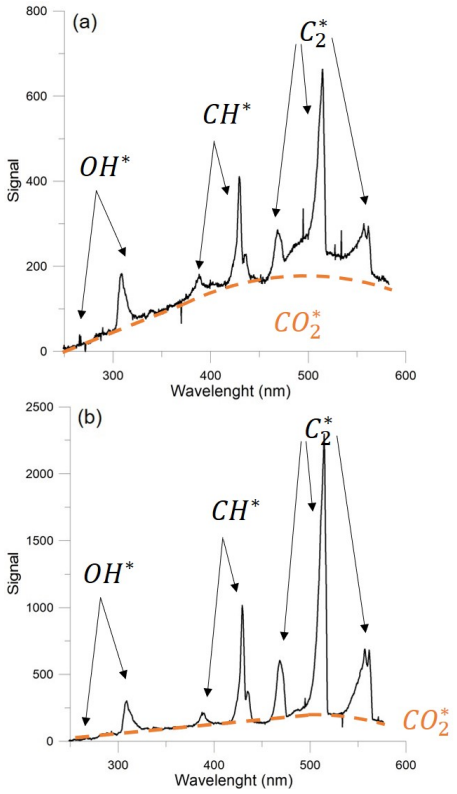

Figure 8: Spectrum for tube 1 with the probe in positions (a) A and (b) B (with a slit=0.50 mm)

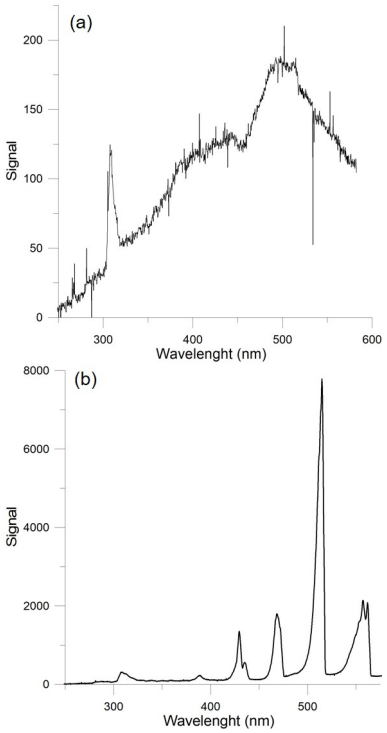

Figure 9: Spectrum for tube 6 with the probe in positions (a) A and (b) B.

5.2.2 Spectroscopy II

After performing the first test, it was concluded that the results of tube 1 were not conclusive enough and the results were better for tube 6 regarding flame emission spectra, so it was decided not to perform further tests with tube 1, focusing only on tube 6 for the next tests.

Focusing on the flame from tube 6, it was decided to deepen the chemiluminescence study in this flame. For that purpose, four different probe positions were considered, three of them in the plume and the other one in the base of the flame, as it is possible to see in Figure 10. For each position, three different slits (0.20, 0.25, 0.50 mm) were used to see if the results obtained were different. The data collection time remained at 50 s.

In Figure 10 it is possible do observe this four positions numbered from 1 to 4.

The results showed that there were no differences when using different slits at each probe position, proving that there were no influence of the slits on the results. For that reason, the figures shown below only present results for the slit=0.5 mm and the last test was performed with a slit equals to 0.5 mm.

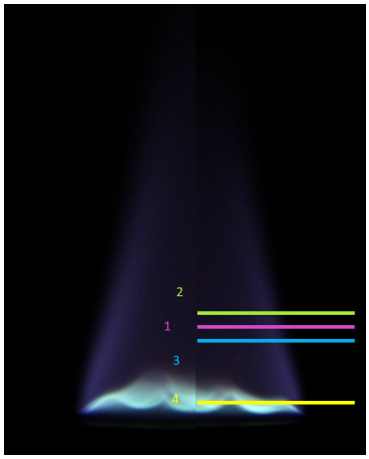

Figure 10: Optical probe at position (a) 1, (b) 2, (c) 3 and (d) 4.

As it is possible to see in figures 11 and 12, in fact, probe positions 1, 2 and 3 are not the best to perform this analysis, with a great contribution of CO_2^* broadband background radiation and, consequently, no conclusions for the equivalence ratio. The same does not occur for probe position 4, presenting conclusive results for the equivalence ratio, only considering CH^*/C_2^* and C_2^*/OH^* ratios. This is because the OH^*/CH^* ratio is characteristic of lean flames and the flame resulting from these tests is rich.

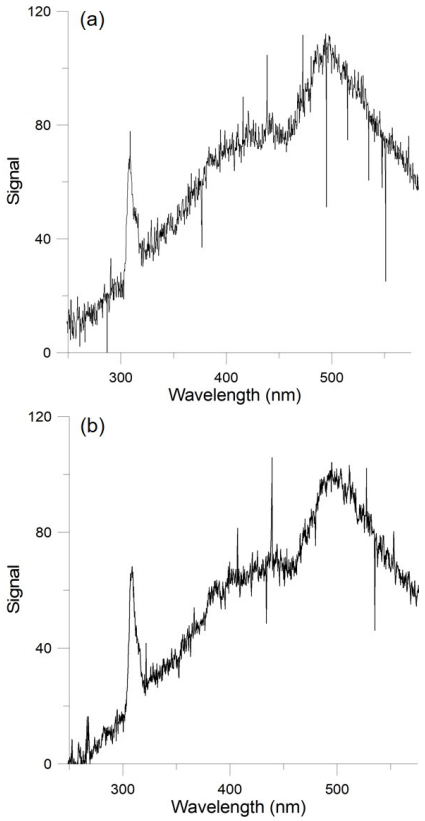

Figure 11: Spectrum for tube 6 with the probe in positions (a) 1 and (b) 2, with a slit=0,5 mm.

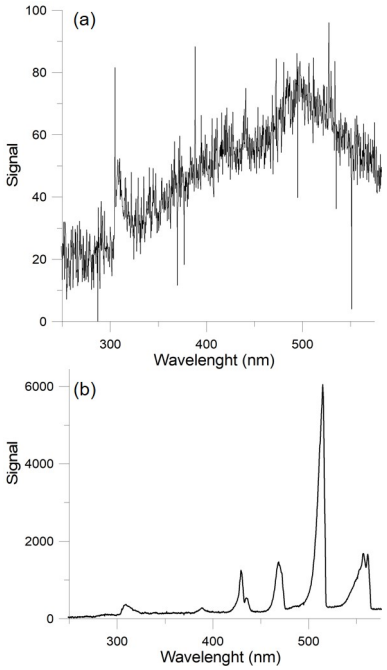

Figure 12: Spectrum for tube 6 with the probe in positions (a) 3 and (b) 4, with a slit=0,5 mm.

5.2.3 Spectroscopy III

In this last test, the spectroscopy analysis was performed only at tube 6 and the data collection time was increased to 300 s, in order to obtain a better estimate for the equivalence ratio. The only probe position considered was the position 4, which allowed to achieve a more reliable estimate of the equivalence ratio in previous tests. This test was performed three times to ensure data repeatability and the results verified were the same.

To calculate the value of the equivalence ratio through the ratios, it was necessary to use calibration curves. A reference flame from a Bunsen burner with propane-air mixture were considered and a calibration equation was obtained for each equivalence ratio.

This estimated value for the equivalence ratio, $\phi = 1.44$, will be useful in the model for the calculation of primary air entrained and could be concluded form Figure 13.

5.3. Thermography analysis

The main goal of this analysis was to find the temperatures verified at the tube entrance (1) and at the end (2), where the flame was anchored, allowing the input of these values into the mathematical model.

As explained in section 4.3, temperatures were recorded using an infrared camera and the data recorded and processed with the camera software, registering the temperature variation over 300s.

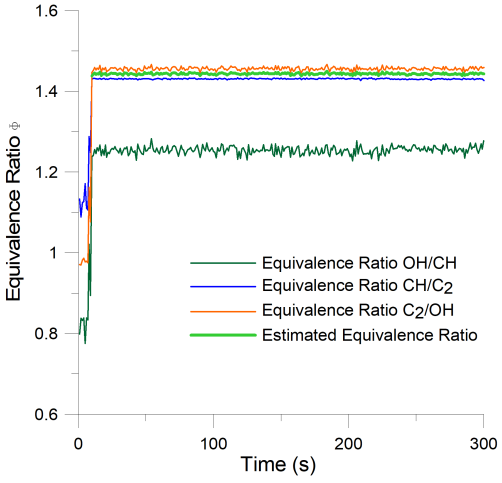

Figure 13: Estimated equivalence ratio for the tube 6.

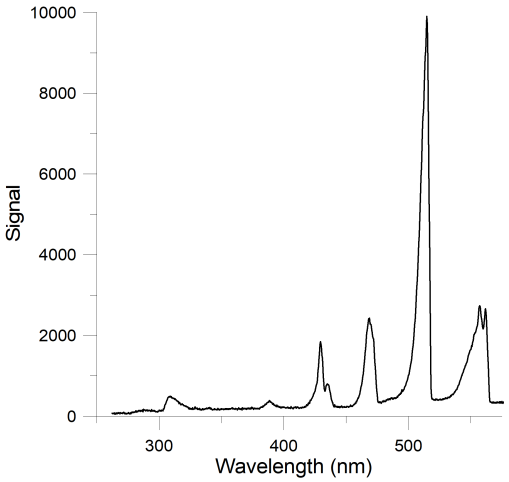

Figure 14: Spectrum for tube 6 at position 4.

As observed in Figure 15, the temperatures registered was, approximately, 125 °C at the end of the tube (2) and 77 °C at the tube entrance (1).

These values for tube temperature will be useful for the calculation of primary air entrained, as an input of the mathematical model.

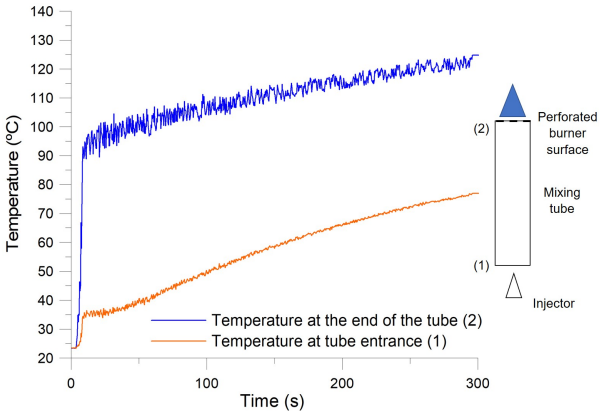

Figure 15: Thermography results recorded in tube 6 during a period of 300 s.

5.4. Mathematical Model

Due to the approximations made in the development of the mathematical model, it was decided to follow a qualitative approach in the analysis of the results.

As the objective was to reach a value for the primary air entrained, after deriving Equation 1, an algorithm was developed in Mat Lab to solve it, in order to discover this unknown. All other variables were known and then these inputs introduced in the algorithm.

With this mathematical model it was possible to study the relations between the different variables considered. Changing the diameter and keeping the

tube temperature, there is a variation of entrained air with variation of the tube diameter. Primary entrained air increases with increasing diameter, contrary to what happens with the equivalence ratio, that decreases.

6. Conclusions

Two different analysis was made on brass, copper, stainless steel, alumina and silicon carbide, using Cambridge Engineering Software and Simapro, to accomplish which of these materials might be most appropriate for the intended purpose. It has been concluded from here that it can be difficult to combine all the important characteristics into one material with reduced impact in the environment, given that, according to CES analysis, the best material would be silicon carbide, and according to LCA analysis would be alumina.

It was very important to know what kind of flames resulted from different geometries and materials used in burners, due to the impossibility of carrying out stability tests. In spectroscopy tests, the results were more conclusive for the tube with larger diameter, using slits and in a position as close as possible to the burner surface. With spectroscopy analysis and with a reference flame from a Bunsen burner with propane-air mixture, a calibration equation was obtained for each ratio, allowing to estimate the equivalence ratio, which was found to be above 1, being the flame rich. From the thermography analysis, temperatures were obtained from both ends of the tube.

Since the temperatures of the two extremities of the tube increase in the same way, the equivalence ratio remains approximately constant during the same period of time and a rich regime occurred, it was believed that the entrained air does not change with increasing temperature and buoyancy has a greater influence, overlapping to the effect of the heat transfer through the material.

A value for primary air entrainment was obtained through the model, although there is a limitation of this model for the different materials considered, and it is not possible to input this data in the model. As future work, some improvements must be made to the model in order to include the entire geometry of the tube.

References

[1] Mário Costa and Pedro Coelho. *Combustão*. Orion, 2012.

[2] Shuhn-Shyurng Hou, Chien-Ying Lee, and Ta-Hui Lin. Efficiency and emissions of a new domestic gas burner with a swirling flame. *Energy Conversion and Management*, 48(5):1401–1410, 2007.

[3] Sumrerng Jugjai and Natthawut Rungsimuntuchart. High efficiency heat-recirculating domestic gas burners. *Experimental thermal and fluid science*, 26(5): 581–592, 2002.

[4] A Namkhat and S Jugjai. Primary air entrainment characteristics for a self-aspirating burner: Model and experiments. *Energy*, 35 (4):1701–1708, 2010.

[5] HS Zhen, J Miao, CW Leung, CS Cheung, and ZH Huang. A study on the effects of air preheat on the combustion and heat transfer characteristics of bunsen flames. *Fuel*, 184:50–58, 2016.

[6] James R Maughan, James R Cahoe, and Reza Ghassemzadeh. Autoregulation of primary aeration for atmospheric burners, April 14 1992. US Patent 5,104,311.

[7] Granta Material Intelligence. URL `http://www.grantadesign.com/`. Accessed in 18-12-2016.

[8] Mark Goedkoop, Anne De Schryver, Michiel Oele, Sipke Durksz, and Douwe de Roest. Introduction to lca with simapro. *PRé Consultants*, 2010.

[9] MJ Goedkoop, R Heijungs, M Huijbregts, A De Schryver, JVZR Struijs, R Van Zelm, et al. A life cycle impact assessment method which comprises harmonised category indicators at the midpoint and the endpoint level. report i: Characterisation. *Den Haag*, 2009.

[10] Christos Keramiotis, Björn Stelzner, Dimosthenis Trimis, and Maria Founti. Porous burners for low emission combustion: An experimental investigation. *Energy*, 45(1):213–219, 2012.

[11] Yunus A Cengel, Robert H Turner, John M Cimbala, and Mehmet Kanoglu. *Fundamentals of thermal-fluid sciences*. McGraw-Hill New York, NY, 2008.